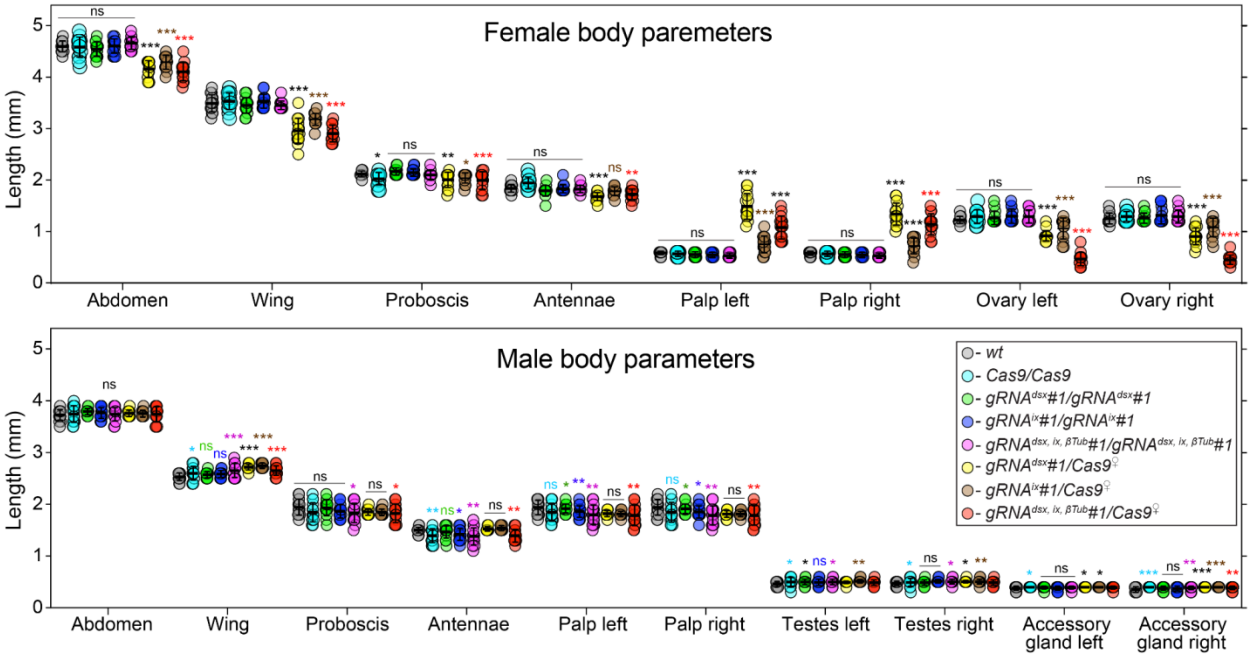

Supplementary Figure 1. Changes in morphological structures induced by disruption of targeted genes. External and internal structures were measured in mosquitoes of each genotype and sex. The trans-hemizygous mosquitoes harboring the maternal *Cas9* (*Cas9*♀) were used for all measurements. The plot shows means and ± SD over fifteen mosquitoes (n = 15) for each morphological structure. All data can be found in Supplementary Table 2. Statistical significance of mean differences was estimated using a two-sided Student's *t* test with equal variance. ($p \geq 0.05^{ns}$, $p < 0.05$*, $p < 0.01$**, and $p < 0.001$***). Source data is provided as a Source Data File.

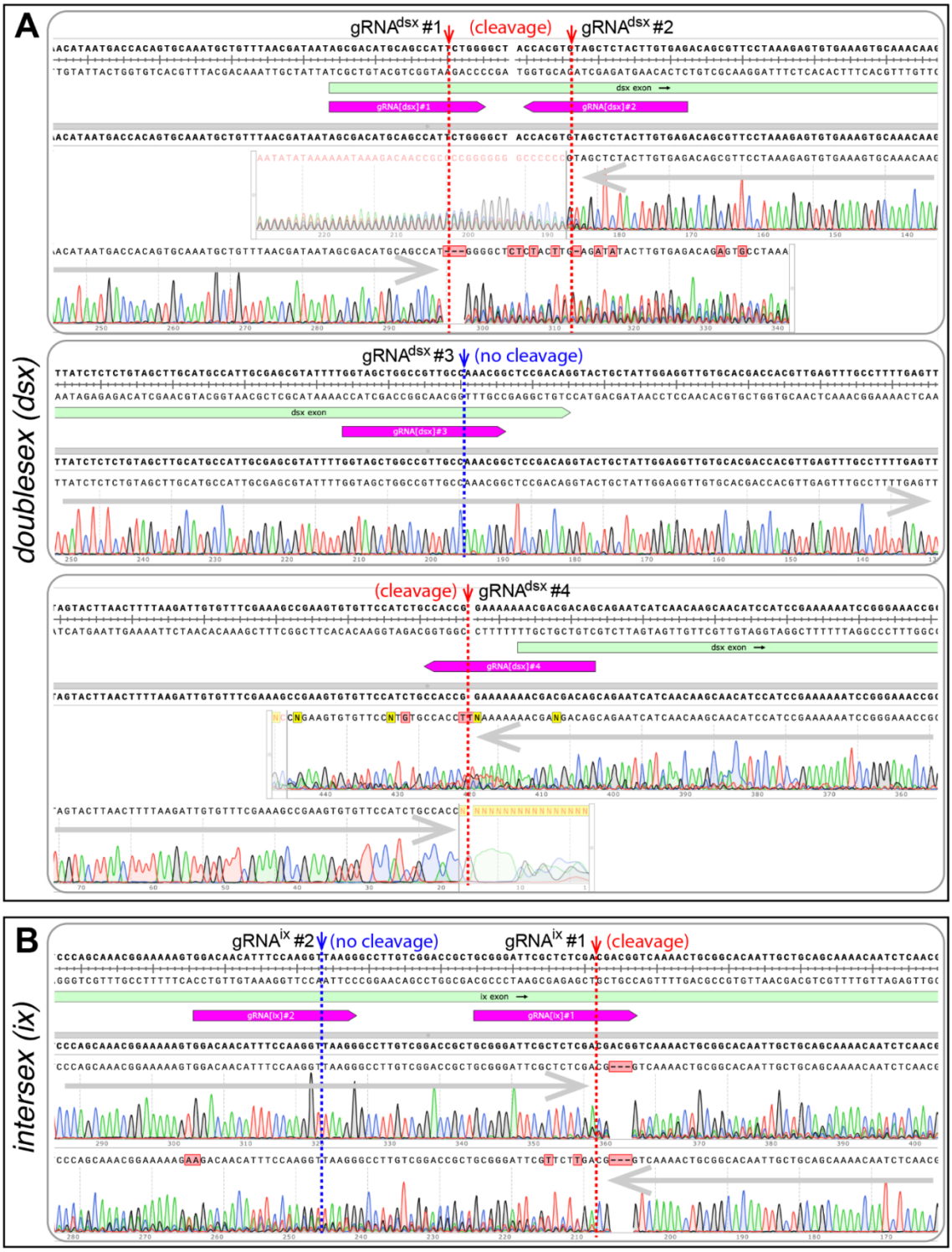

Supplementary Figure 2. Induced mutations at the targeted sequences in *dsx* and *ix*. The gene sequences targeted by gRNAs were PCR amplified from pgSIT mosquitoes and Sanger sequenced. Good quality of Sanger read chromatogram indicates the presence of a single consistent temple sequence (no cleave) at a targeted region, for example *gRNA^{dsx}#3* (**A**) or *gRNA^{is}#2* (**B**). An active CRISPR/gRNA-mediated cleavage at a particular DNA target results in re-ligation of cut fragments leading to the origin of diverse mutation-bearing alleles. These induced mutations are localized around the gRNA cleavage site and result in the drop of Sanger read quality (cleavage) as indicated for *gRNA^{dsx}#1*, *gRNA^{dsx}#2*, *gRNA^{dsx}#4*, (**A**) and *gRNA^{is}#1* (**B**).

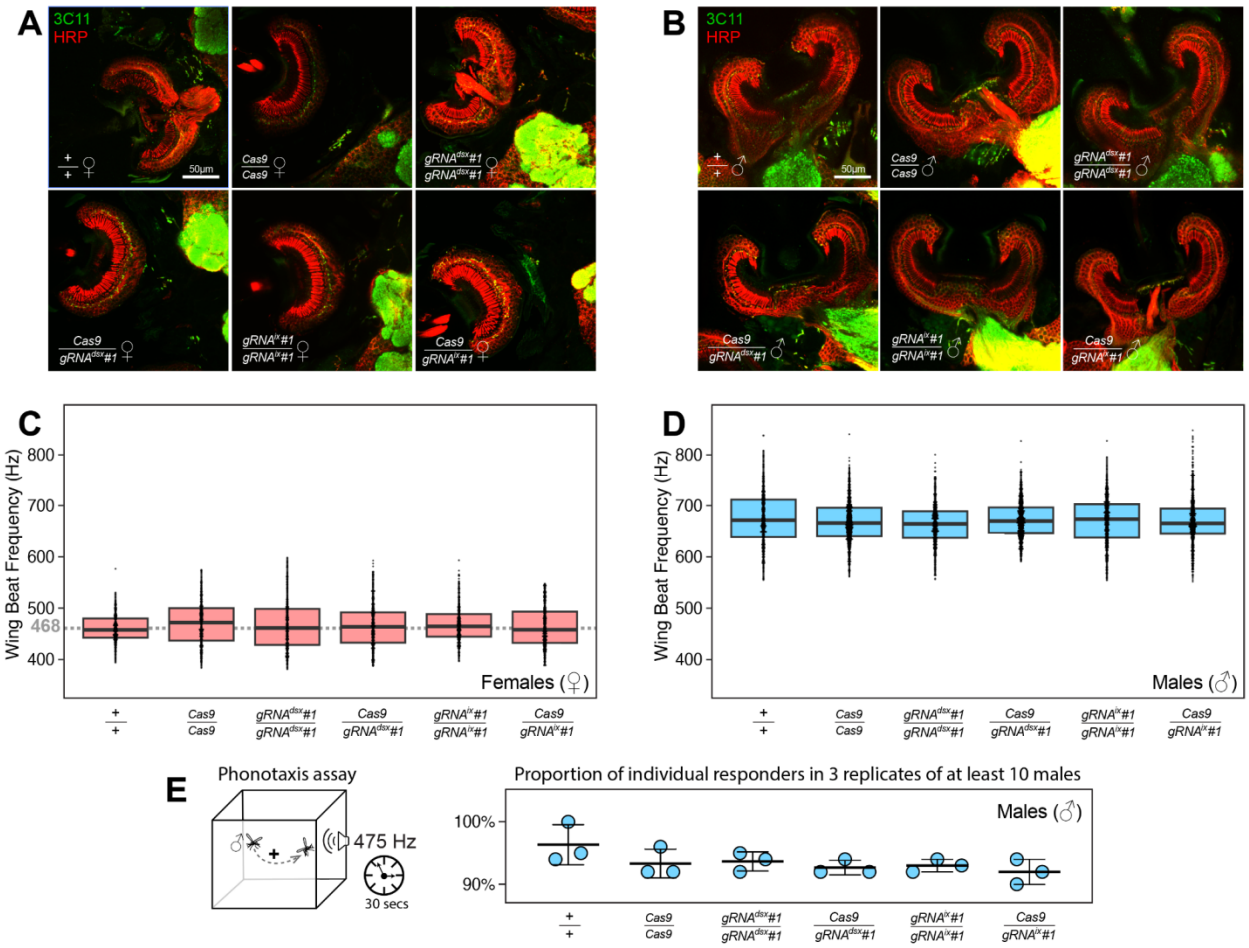

Supplementary Figure 3. *Ae. aegypti dsx* or *ix* disruption does not result in significant alterations in ear anatomy, Wing Beat Frequency (WBF), and male phonotactic behaviors. Immunohistochemistry and microanatomic comparison of mosquito Johnston's Orgran (cup-like structure) with chordotonal neurons responsible for auditory transduction in females (♀'s, **A**) or males (♂'s, **B**) among different genotypes. Female JO's contained far fewer neurons than males across all genotypes, and distributions of synaptic punctate assessed by Anti-Synapsin (3C11, in green) were restricted to the somata, as opposed to the male-type distribution observable in the gap between the cilia and somata tracked by anti-Horseradish Peroxidase (HRP, in red). WBFs are different between *Ae. aegypti* ♀'s and ♂'s, and are shown on separate plots, (**C**) and (**D**) respectively. Each point represents the estimated frequency of a single fly-by (aka. the frequency of sound produced by one event of a mosquito flying past the microphone). WBF box plots indicate the median (middle bar), and 25% and 75% quartiles (lower/upper boundaries of box). The average ♀ WBF is 468 Hz. No significant differences were observed between ♀ groups, or between ♂ groups, regardless of the genotypes tested (ANOVA on ranks, $P > 0.05$). The male phonotaxis assay was conducted, in which individual flying ♂'s showed attractive or no response (scored as 1 or 0, respectively) toward the female-specific WBF produced for 30 secs by a speaker (**E**). Three batches (aka. 3 replicate groups) of at least 10 ♂'s were examined for each genotype. ♂'s across all genotypes exhibited robust responses to sound. The point plot shows the mean (middle bar) and one Standard Deviation (± SD) for the proportion of ♂'s responding to the auditory stimulus. No significant differences were observed across groups (*Chi*-squared test, $P > 0.05$).

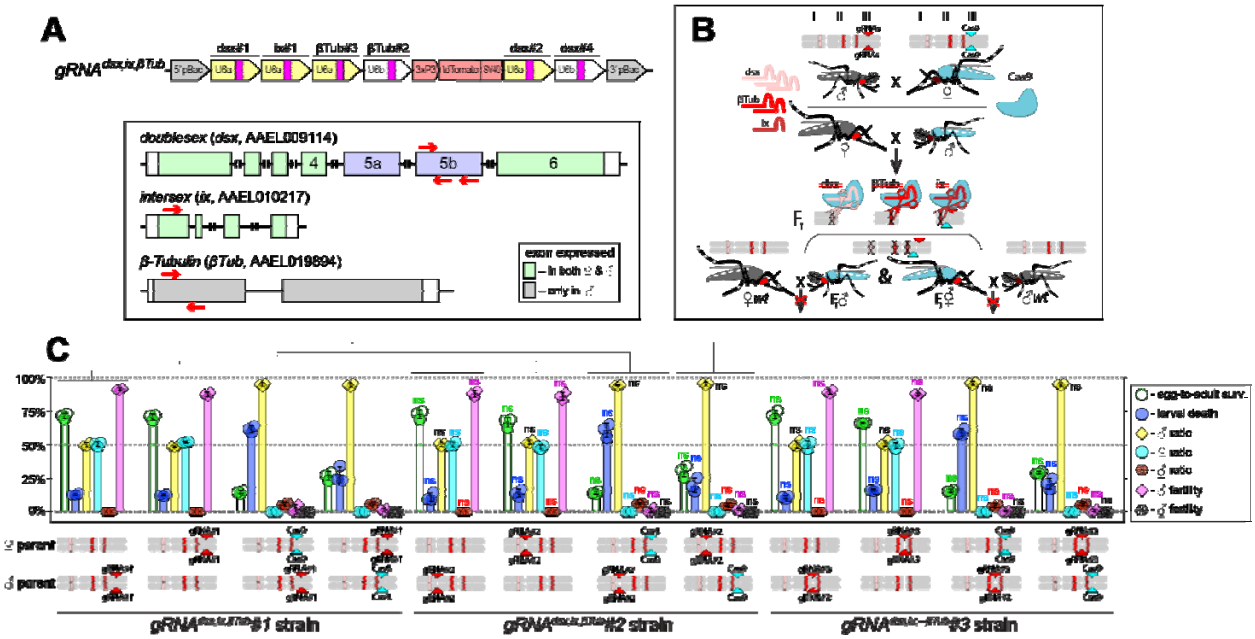

Supplementary Figure 4. Genetic Characterization of independent transgenic strains for CRISPR/Cas9-mediated disruption of *dsx, ix,* and *βTub.* (**A**) Schematic maps of targeted genes (box) and $gRNA^{dsx,ix,\beta Tub}$ construct. Relative locations of gRNA target sequences are depicted with red arrows (box). $gRNA^{dsx,ix,\beta Tub}$ harbors a *3xP3-tdTomato* marker and six gRNAs to guide the simultaneous CRISPR/Cas9-mediated disruption of *dsx*, *ix*, and *βTub* genes. (**B**) A schematic of the reciprocal genetic cross between the homozygous *Cas9*, marked with *Opie2-CFP*, and homozygous $gRNA^{dsx,ix,\beta Tub}$*#1* to generate the trans-hemizygous F_1 (aka. pgSIT) progeny. Relative positions of *dsx*, *ix*, and *βTub* genes (bar's color corresponds to gRNA's color), and transgene insertions in the *Cas9* (*Nup50-Cas9* strain) and $gRNA^{dsx,ix,\beta Tub}$*#1* strains are indicated in the three pairs of *Ae. aegypti* chromosomes. (**C**) Three independent $gRNA^{dsx,ix,\beta Tub}$ strains were generated and assessed by crossing to the *Cas9* strain and comparing the pgSIT phenotypes induced in each trans-hemizygous progenies. The survival, sex ratio, and fertility of trans-hemizygous and hemizygous $gRNA^{dsx,ix,\beta Tub}$ mosquitoes were scored for each of three $gRNA^{dsx,ix,\beta Tub}$ strains and compared to the corresponding values found for $gRNA^{dsx,ix,\beta Tub}$*#1* strain. The bar plot shows means and ± SD over triple biological replicates (n = 3, all data can be found in Supplementary Table 4). The bars show means and ± SD over three biologically independent groups of 50 WT ♀'s (n = 3) for each experimental condition. Statistical significance of mean differences was estimated using a two-sided Student's *t* test with equal variance. ($p \geq 0.05^{ns}$, $p < 0.05$*, $p < 0.01$**, and $p < 0.001$***). Source data is provided as a Source Data File.

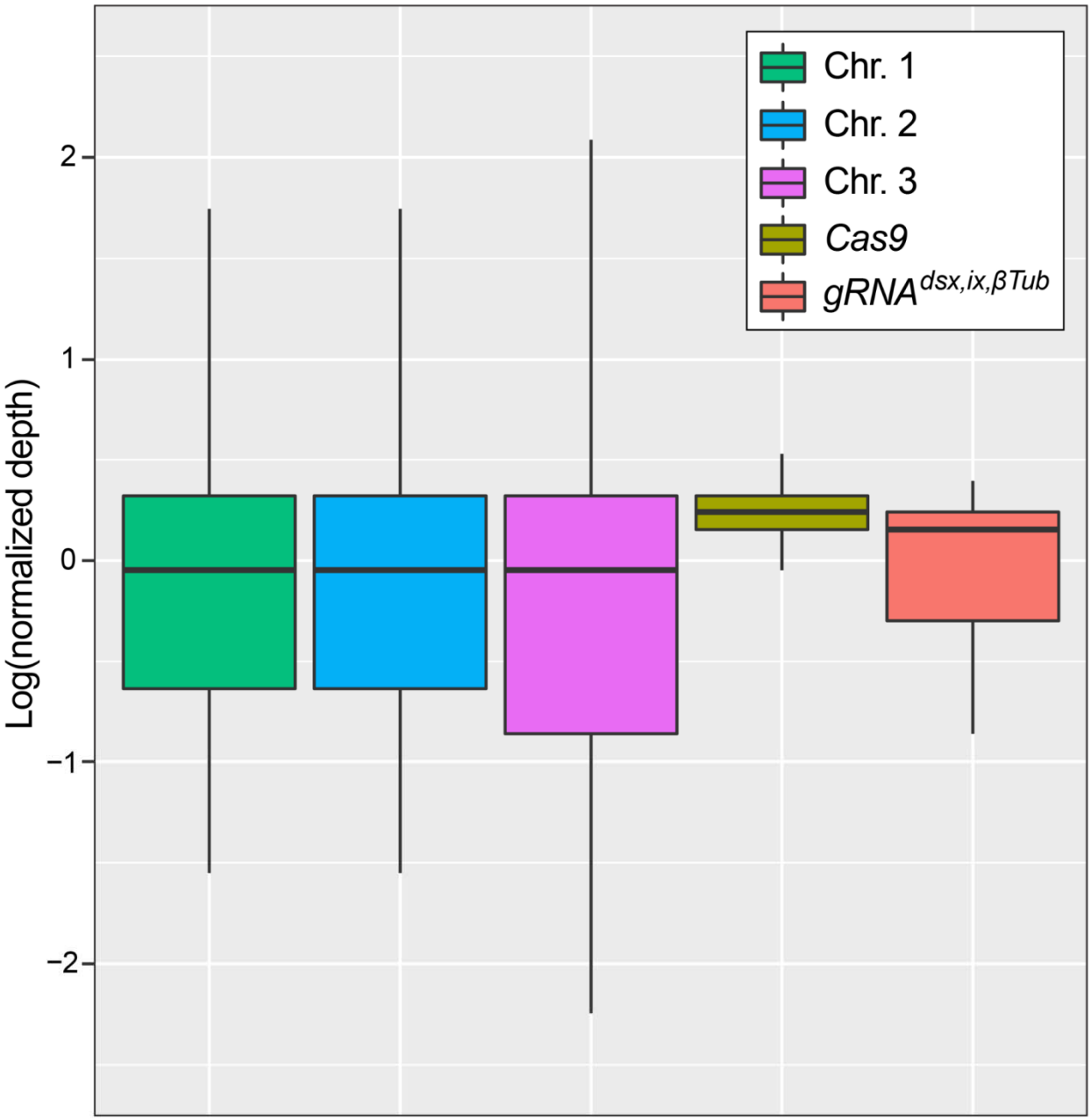

Supplementary Figure 5. Determination of transgene copy number for the *gRNA*$^{dsx,ix,\beta Tub}$*#1* strain using Oxford Nanopore genome sequencing. tandard box plot depicting the coverage distributions of the three chromosomes and the *Cas9* and *gRNA*$^{dsx,ix,\beta Tub}$ transgenes in trans-hemizygous *gRNA*$^{dsx,ix,\beta Tub}$*#1/Cas9* (aka. pgSIT) mosquitoes. The center line is median, first and third quartiles are the bounds of the box, upper and lower whiskers extend from the box to the largest and lowest observed value, but no further than 1.5* Interquartile Range (IQR) from the box. Sequencing depths for chromosomes 1, 2, 3 and for Cas9 and *gRNA*$^{dsx,ix,\beta Tub}$ transgenes were 9.71, 9.47, 9.17, 12.23, 9.50, respectively. Normalized sequencing depths were 1.03, 1.00, 0.97, 1.30, 1.01 consistent with the transgenes being present at single copy. The Nanopore sequencing data have been deposited to the NCBI sequence read archive (SRA) under BioProject ID PRJNA942966 and BioSample ID SAMN33705934.

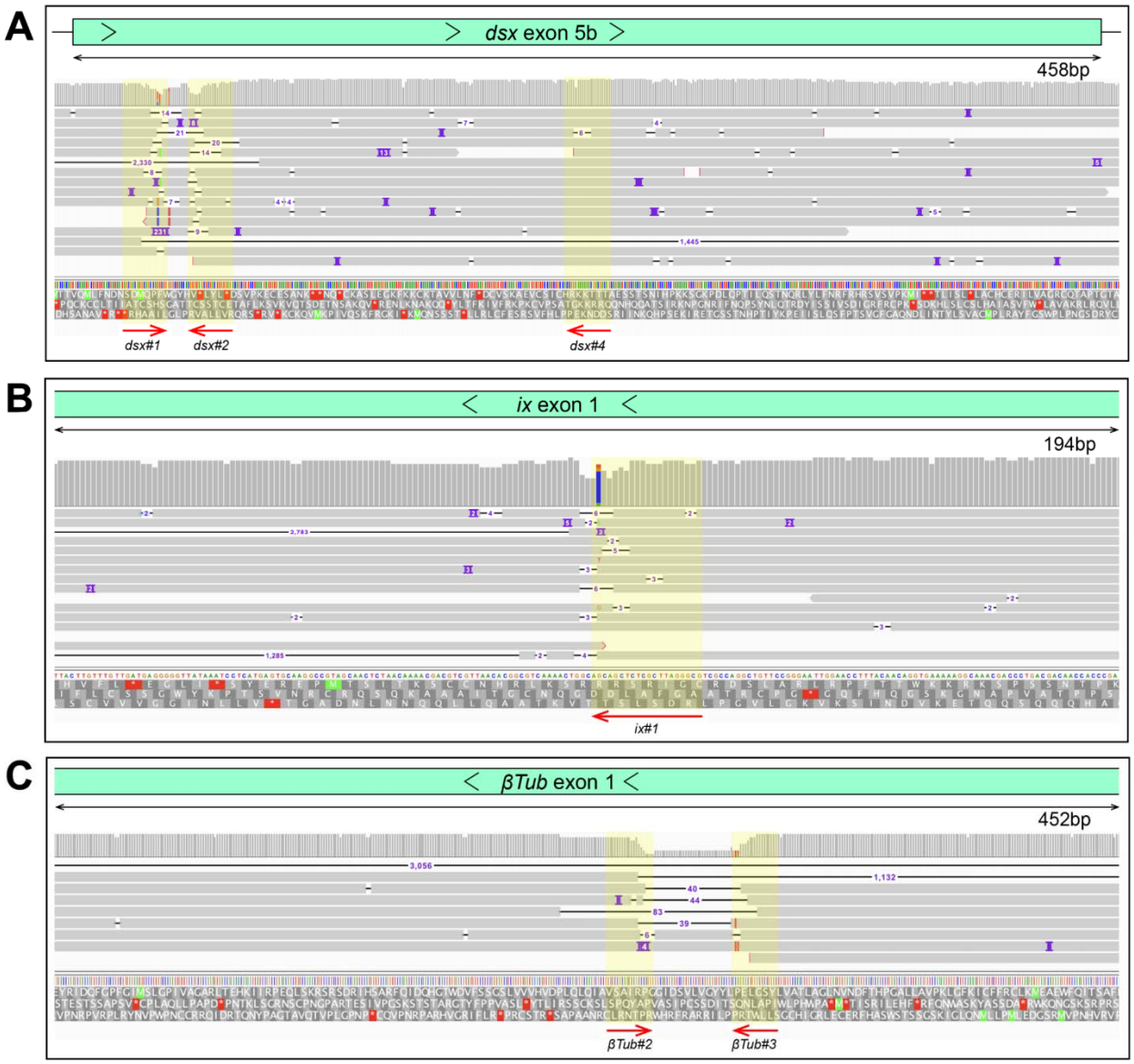

Supplementary Figure 6. Oxford Nanopore sequencing results validating disruptions in the target sites. Integrated genome browser snapshots are zoomed in at genome regions containing gRNA target sites at *dsx* (**A**), *ix* (**B**), and *βTub* (**C**) genes in pgSIT ♂'s and ♀'s. The direction of DNA strand and scale is indicated above generated reads. Sampled deletion mutations localize to gRNA target sites (yellow overlay) (**A**).

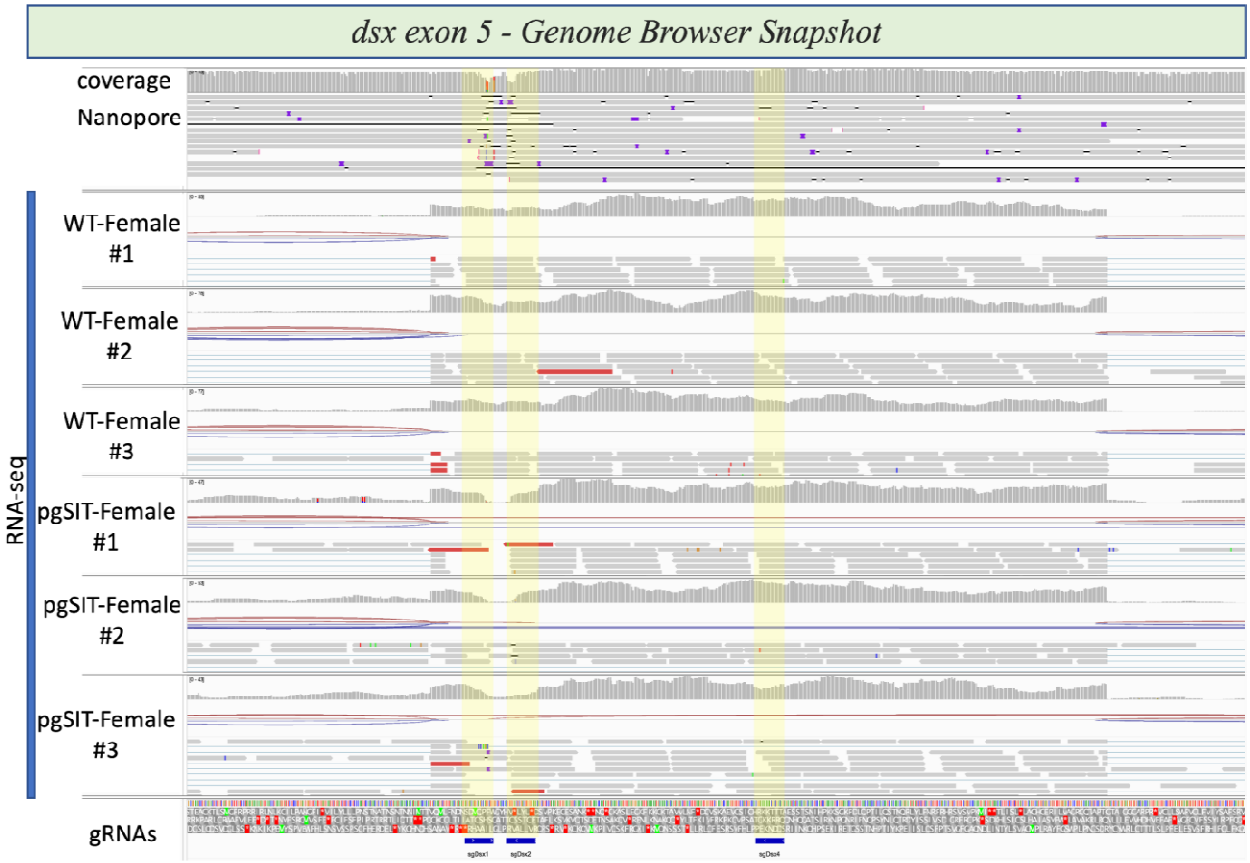

Supplementary Figure 7. Integrative genome browser snapshot of *dsx* validating gRNA target disruption in both the DNA and RNA. Oxford Nanopore reads are aligned on the top and RNAseq reads for the various genotypes indicated are aligned. On the bottom in blue are the gRNA target sites.

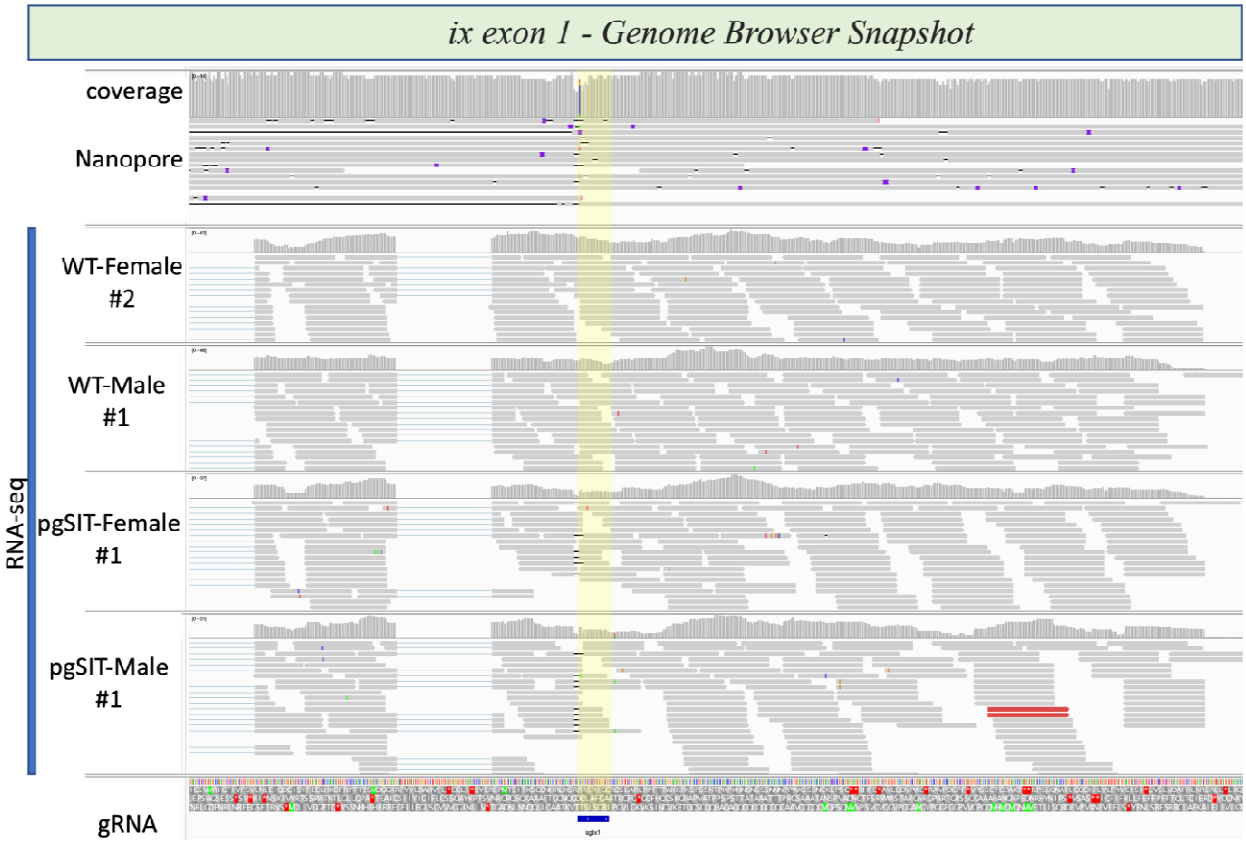

Supplementary Figure 8. Integrative genome browser snapshot of *ix* validating gRNA target disruption in both the DNA and RNA. Oxford Nanopore reads are aligned on the top and RNAseq reads for the various genotypes indicated are aligned. On the bottom in blue is the gRNA target site.

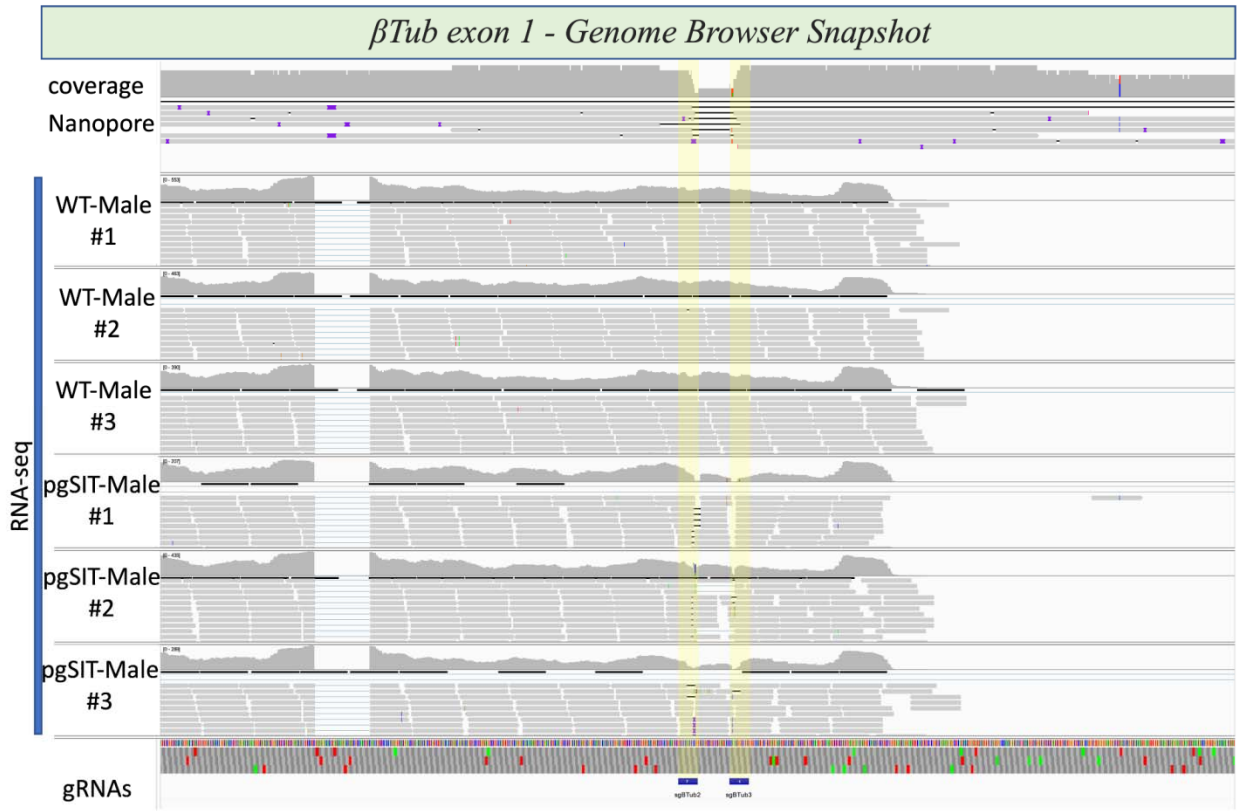

Supplementary Figure 9. Integrative genome browser snapshot of *βTub* validating gRNA target disruption in both the DNA and RNA. Oxford Nanopore reads are aligned on the top and RNAseq reads for the various genotypes indicated are aligned. On the bottom in blue are the gRNA target sites.

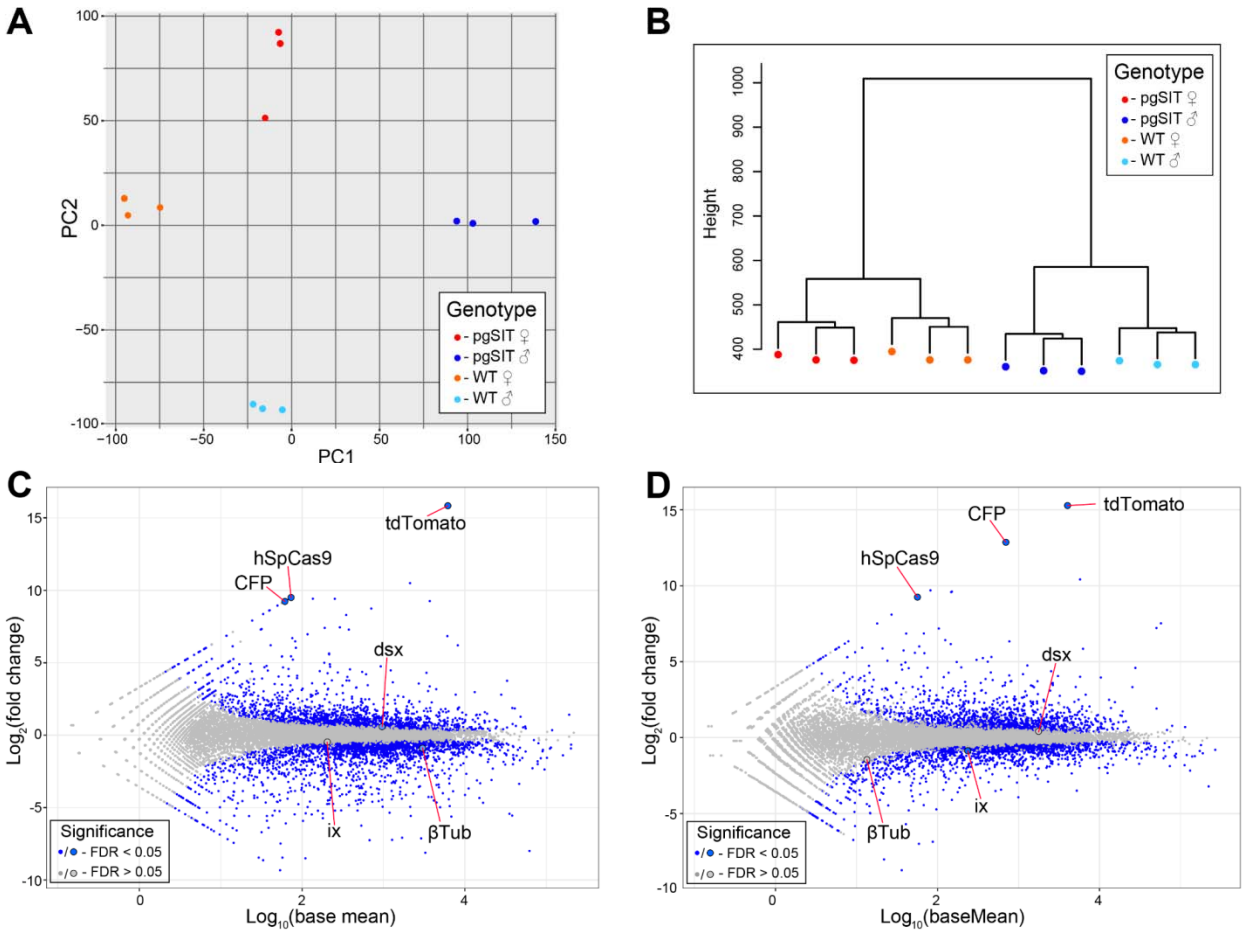

Supplementary Figure 10. Transcription profiling and expression analysis of *Ae. aegypti* liverpool and pgSIT mosquito samples. (**A**) PCA analysis and **(B)** hierarchical clustering of twelve samples used for RNA sequencing. MA-plots showing the differential expression patterns between: **(C)** pgSIT ♂'s vs WT ♂'s, and **(D)** pgSIT ♀'s vs WT ♀'s. Blue bots indicate significantly differentially expressed genes (FDR < 0.05), while non-significantly differentially expressed genes are indicated by gray dots (FDR > 0.05). Targeted and transgenic genes are depicted by the larger blue or gray dots.

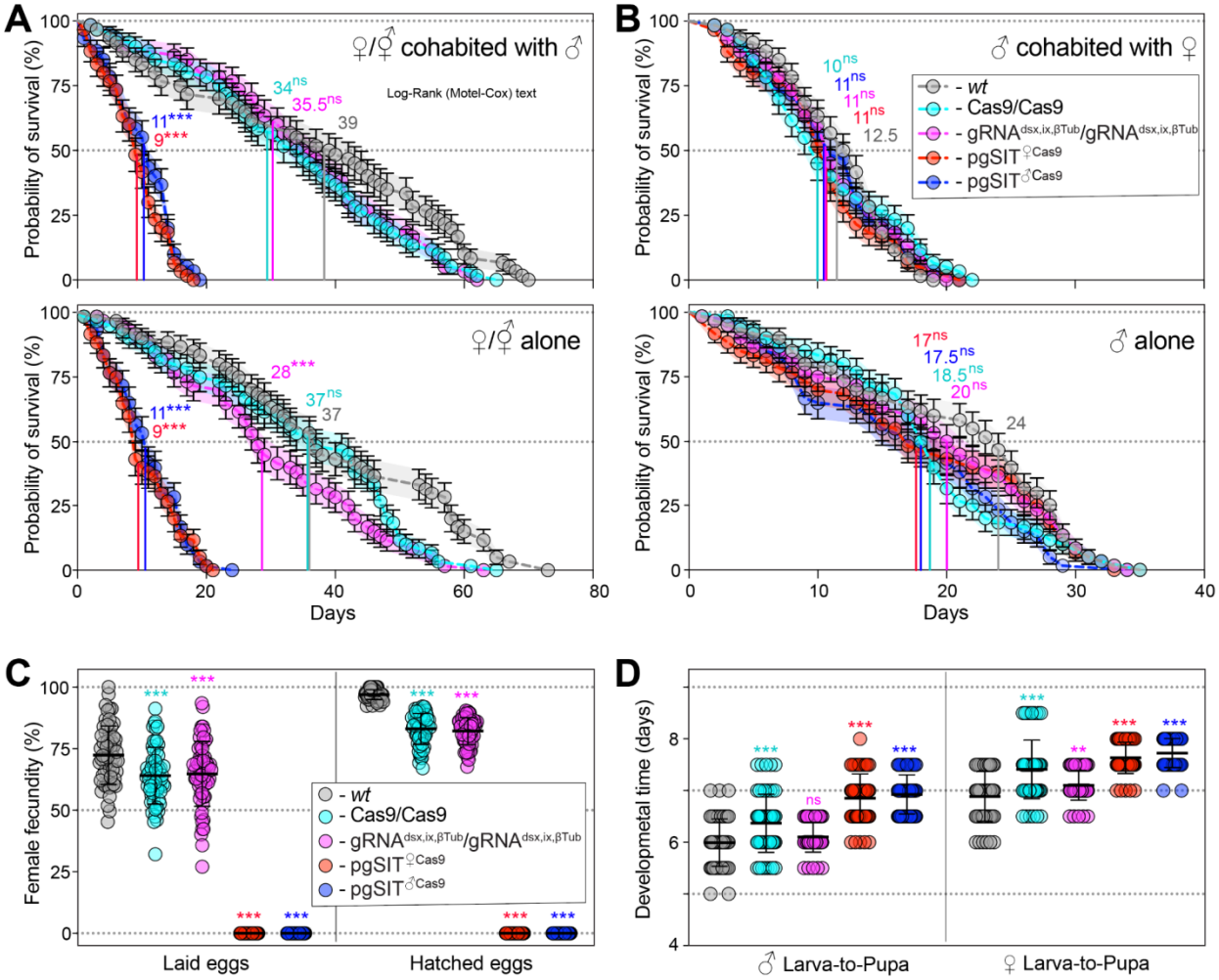

Supplementary Figure 11. Longevity, fecundity, and developmental times of the generated pgSIT mosquitoes. (**A**) Survival plots of 20 adult ♀'s or ⚲'s either cohabitated with ♂'s or not, and (**B**) 20 adult ♂'s either cohabitated with ♀'s or not over three independent experiments (n=3). Survival means ± standard errors (SE) over days following adult eclosion are plotted. Vertical lines and values present median survivals for each tested group. Mosquito survival curves for each tested group were compared to the curve for WT's mosquitoes of the corresponding sex. The departure significance was assessed with the Log-rank (Mantel-Cox) test and is indicated above median values. (**C**) Female fecundity plots, measured as egg laying and hatching rates, of 60 adult ♀'s or ⚲'s of each tested group (n = 60). (**D**) Plots of larva-to-pupa and pupa-to-adult developmental times were measured in 60 ♂'s and ♀'s or ⚲'s for each tested group (n = 60). Both point plots in panels **C** and **D** show mean and ± SD (Supplemental Table 7). Statistical significance of mean differences was estimated using a two-sided Student's *t* test with equal variance.($p \geq 0.05^{ns}$, $p < 0.05$*, $p < 0.01$**, and $p < 0.001$***). Source data is provided as a Source Data File.

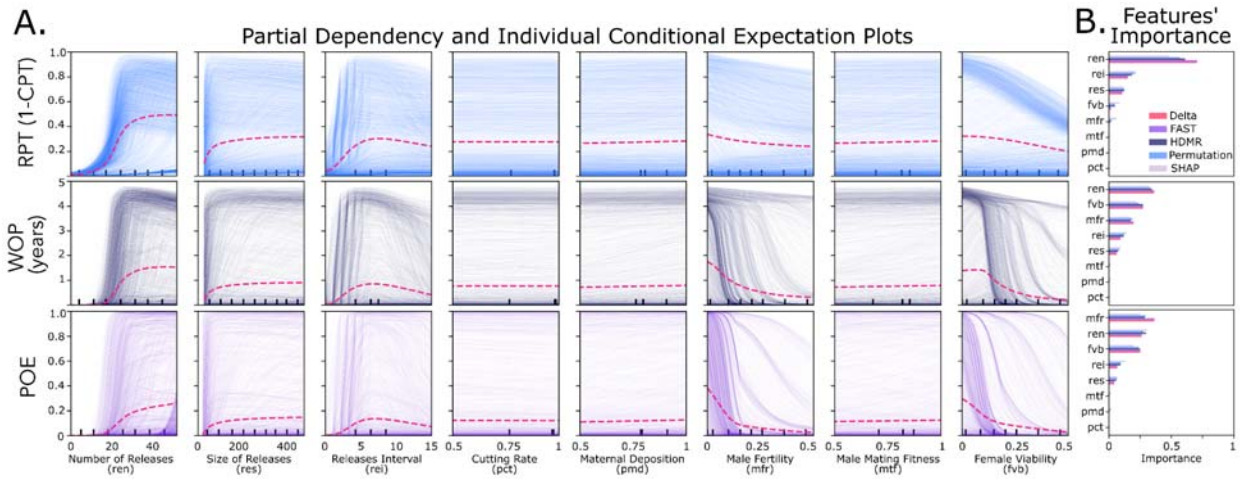

Supplementary Figure 12. Sensitivity of pgSIT population suppression outcomes to model parameters. A Partial dependency (thin traces) and individual conditional expectation plots[3] (magenta dashed lines) are depicted for regression models fitted to three model outcomes: i) probability of elimination (POE), ii) window of protection (WOP) (measured in years), and iii) reduction in cumulative potential for transmission (RPT). These three outcomes were evaluated for several parameters - number of releases, size of releases (as a proportion of the number of wild adults in the environment), release interval (in days), gRNA cutting rate, Cas9 maternal deposition rate, male fertility, male mating competitiveness (relative to wild-type males), and female viability. Population suppression outcomes are most sensitive to release schedule parameters (number, size and interval of releases), male fertility and female viability. **B** Statistical sensitivity analysis metrics on the simulated data are compared to importance metrics for surrogate models. For the first-order statistical sensitivity analysis, we used Delta[4], Fourier Amplitude Sensitivity Test (FAST)[5], and High-Dimensional Model Representation (HDMR)[6]; whilst for the emulators we used Permutation feature importance[7], and SHapley Additive exPlanations (SHAP)[8]. The normalized importance barcharts are in good agreement with the variable-to-outcome rankings. (Supplementary Tables 10-11). Source data are provided as a Source Data File.

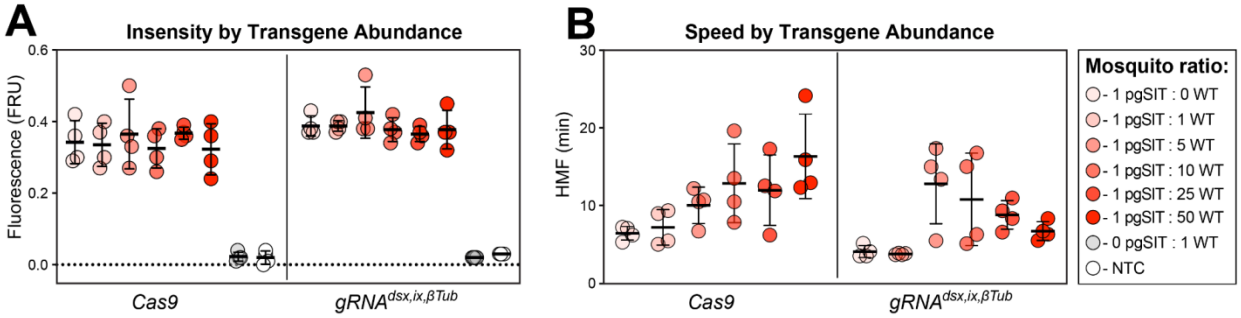

Supplementary Figure 13. Sensitive and rapid detection of transgenic DNA fragments with the Sensitive Enzymatic Nucleic acid Sequence Reporter (SENSR) assay. (**A**) Intensity of signal from SENSR assay for both *Cas9* and *gRNA*$^{dsx,ix,\beta Tub}$ constructs along a concentration gradient, as ratio of *pgSIT*$^{♀Cas9}$ to WT mosquitoes, and No Template Control (NTP). The fluorescence signal represents the background-subtracted signal (n = 4). (**B**) Speed of cleavage along a ratio of *pgSIT*$^{♀Cas9}$ to WT mosquitoes, as target abundance. The speed of collateral activity is represented using an HMF analysis (n = 4). (Supplementary Tables 12-13). Source data is provided as a Source Data File.

References

1. Li, M. *et al*. Suppressing mosquito populations with precision guided sterile males. *Nature Communications* vol. 12 Preprint at https://doi.org/10.1038/s41467-021-25421-w (2021).

2. Héctor M. Sánchez C., Sean L. Wu, Jared B. Bennett, John M. Marshall. MGDrivE: A modular simulation framework for the spread of gene drives through spatially explicit mosquito populations. *Methods in Ecology and Evolution* (2019) doi:10.1111/2041-210X.13318.

3. Molnar, C. *Interpretable Machine Learning*. (Lulu.com, 2020).

4. A new uncertainty importance measure. *Reliab. Eng. Syst. Saf.* **92**, 771–784 (2007).

5. Cukier, R. I., Fortuin, C. M., Shuler, K. E., Petschek, A. G. & Schaibly, J. H. Study of the sensitivity of coupled reaction systems to uncertainties in rate coefficients. I Theory. *J. Chem. Phys.* **59**, 3873 (2003).

6. Saltelli, A., Tarantola, S. & Chan, K. P.-S. A quantitative model-independent method for global sensitivity analysis of model output. *Technometrics* **41**, 39–56 (1999).

7. Breiman, L. Random Forests. *Mach. Learn.* **45**, 5–32 (2001).

8. Lundberg and Su-In Lee, S. A Unified Approach to Interpreting Model Predictions. https://proceedings.neurips.cc/paper_files/paper/2017/file/8a20a8621978632d76c43dfd28b67767-Paper.pdf.